

Study on characteristics of co-pyrolysis of biomass and oil-based drill cuttings from shale gas development

Boxun Zhou, Manzoor Sanjrani, Shici Zhang, Hongli Diao, Yanyun Wang, Siyu Huang, Qi Liu, Shibin Xia*

School of Resources and Environmental Engineering, Wuhan University of Technology, Wuhan 430070, China, emails: xiashibin@126.com (S.B. Xia), boxunzhou@foxmail.com (B.X. Zhou), manzoor.geo@gmail.com (M. Sanjrani), zhangshici@whut.edu.cn (S.C. Zhang), hongli.diao@aliyun.com (H.L. Diao), 846324624@qq.com (Y.Y. Wang), hsy1987@whut.edu.cn (S.Y. Huang), amuliuqi@qq.com (Q. Liu)

Received 23 November 2019; Accepted 11 July 2020

ABSTRACT

Co-pyrolysis of oil-based drill cuttings (ODCs) and biomass (palm fruits) were systematically investigated in this work. Thermogravimetric (TG) analysis was applied to study the pyrolysis characteristics of ODCs and biomass at different heating rates, different temperature ranges, and different mixing ratios. Differential thermogravimetry curves indicate that the co-pyrolysis produces a synergistic effect in 20°C–450°C and above 750°C. Fixed-bed pyrolysis was employed to determine the best pyrolysis parameters and analyze the co-pyrolysis mechanism: when the proportion of ODCs was 70%, the oil content of the pyrolysis residue was 21.71% lower than the calculated value; gas chromatography-mass spectrometry analysis found that when the proportions of ODCs were 70% and 80%, co-pyrolysis could reduce harmful substances and increase favorable substances in liquid yields. Flynn–Wall–Ozawa method and Coats–Redfern integral method was employed to perform a dynamical analysis on TG curves over a temperature range of 20°C–350°C. Both results show that the co-pyrolysis of 5:5 mixtures can reduce pyrolysis activation energy.

Keywords: Oil-based drill cuttings; Biomass; Co-pyrolysis; Shale gas; Oil content

1. Introduction

Shale gas is a promising energy resource with abundant reserves and non-polluting combustion products in China [1]. However, the considerable amount of by-products and wastes generated by the gas industry must be properly managed to avoid environmental risks [2]. During the development of shale gas in Fuling, Chongqing, China, oil-based drilling fluid was utilized for multi-interval fracturing, which was later circulated to the ground with cuttings and mud. After the separation of the liquid phase, the remaining solid phase is called oil-based drill cuttings (ODCs) [1–3]. ODCs are viscous black semi-solids, alkaline, mainly composed of

ground shale, clay, heavy metals, fracturing fluids, petroleum hydrocarbons [4]. Containing high moisture (10%–20%) and oil (6%–40%), ODCs can contaminate the soil, destroy the nutrient environment, thus preventing crop growth, increasing heavy metals and chemical oxygen demand in water [5]. Therefore, effective treatment of ODCs has attracted widespread attention.

Common methods for ODCs disposal include bioremediation, phytoremediation, solidification and stabilization, supercritical fluid extraction, surfactant-enhanced washing, microwave treatment, and pyrolysis [6–12]. Among those, pyrolysis can efficiently remove oil contaminants in ODCs in short treatment time, as the contaminants are mostly volatile or semi-volatile, and instruments for pyrolysis are

* Corresponding author.

of low cost [2,5,11]. Many researchers have studied the effects of pyrolysis temperature, gas atmosphere, pretreatment, and addition of catalysts on the pyrolysis of ODCs [1,13,14]. Nevertheless, the detailed pyrolysis mechanism of ODCs in different temperature ranges is still unclear, while the optimization and utilization of ODCs pyrolysis liquid yield are still to be explored.

Biomass refers to the substances produced by photosynthesis from carbon dioxide and water. Its main components include cellulose, hemicellulose, lignin, a small amount of organic extracts, and ash [15–17]. Biomass resources have the advantages of large reserves, fast growth, low sulfur content and low nitrogen content, and they can be collected from forest or crop residues, industrial organic waste, aquatic plants, human and animal manure [18,19]. However, due to its low energy density, biomass is not easy to utilize. At present, combustion, pyrolysis, and gasification are utilized for biomass thermochemical conversion [15,17,19–22].

The idea of this paper was inspired by studies about the co-pyrolysis of coal and biomass [23–25]. Biomass has a high H/C ratio, while coal is just the opposite. When they are jointly pyrolyzed, the “co-hydrogen” effect can lead to increased yields and improve the quality of pyrolysis oil [26–32]. Also, some studies show that variations in heating rate and mixing ratio of coal and biomass may have a significant impact on the energy consumption of co-pyrolysis [33–35]. Until now, there are few attempts to co-pyrolyze biomass and ODCs. Lin et al. [36] conducted co-pyrolysis of rice husk and oily sludge to analyze their liquid and gas yields, and Shao [37] studied the co-pyrolysis characteristics of alkaline lignin and oil shale. However, either these studies failed to fully explore the characteristics of co-pyrolysis, or they failed to use common and cheap raw materials. Therefore, more experiments are needed to find other suitable biomass types for co-pyrolysis with ODCs, to find better reaction parameters, to systematically analyze the mechanism of co-pyrolysis and changes in activation energy.

Under such a circumstance, we chose palm fruits as biomass materials to study the co-pyrolysis with ODCs. Palm trees are widely planted in China, but their fruits are not edible and generally discarded as waste. Hence, it will be of great significance to explore their potential value in terms of environmental protection and commercial use. In this research, thermogravimetry (TG) analysis was carried out to investigate the law of weight loss at different heating rates and different temperature ranges; fixed bed pyrolysis was applied to determine the best pyrolysis parameters, and to discuss the pyrolysis liquid yields of ODCs and biomass under different mixing ratios. Based on the experiment data, we put forward the co-pyrolysis mechanism analysis of these two materials. In order to further verify the promoting effect of co-pyrolysis, Flynn–Wall–Ozawa (FWO) and Coats–Redfern methods were employed to calculate the pyrolysis activation energy of ODCs, biomass and their mixtures.

2. Material and methods

2.1. Site description and sample preparation

Sinopec Jiangnan Oilfield of Chongqing Fuling Shale Gas Co., Ltd. is located in the eastern part of Chongqing, China, with an east longitude of 106°56′–107°43′, the north

latitude of 29°21′–30°01′, the altitude of 200–800 m. According to the existing geological data and capacity evaluation, the Fuling shale gas field has a resource of 380.6 billion m³. It is the first large shale gas field in China and the largest shale gas field in the world except for North America [38]. During the drilling process, each well can produce 250 m³ ODCs. The on-site treatment of ODCs including desander/vibrating screen, collection, and pyrolysis [1]. The fresh ODCs used in this research were collected directly from well No. 5 of Sinopec Jiangnan Oilfield of Chongqing Fuling Shale Gas Co., Ltd., and sealed in high-density polyethylene barrels.

Palm fruits were collected in Wuhan, Hubei Province, China, with a geographical position of 29°58′–31°22′ north latitude, 113°41′–115°05′ east longitude, less than 50 m altitudes, belonging to the north subtropical monsoon (wet) climate. The palm fruits were washed with distilled water, then baked at 60°C for 12 h, and stored in valve bags.

Before each test, the samples of ODCs and biomass were separately baked at 105°C for 24 h. Some samples were mixed with different weight ratios (2:8, 3:7, 5:5, 7:3, and 8:2), then crushed and mixed with a mortar and passed through a 10-mesh sieve. Treated samples of ODCs and biomass are shown in Fig. 1.

2.2. Characterization

Carbon, hydrogen, nitrogen, sulfur and oxygen analyzer (CHNS/O) (Vario EL cube-type, Elementar Analysis System Co., Germany), X-ray fluorescence (XRF) spectrum analyzer (Zetium, PANalytical. B. Van, Netherlands), and inductively coupled plasma-optical emission spectrometer (Prodigy 7, Leeman Labs Inc., 6 Wentworth Drive, Hudson, NH03051, U.S.A) were used for elemental and chemical components analysis of the ODCs and biomass samples. Gas chromatography-mass spectrometry (GC-MS, Agilent 7890, Agilent Technologies Co., Ltd., 5301 Stevens Creek Blvd., Santa Clara, CA95051, U.S.A) and infrared spectrophotometer (SYT700, Beijing Sunyoung Technology Co., Ltd., No. 3 Moli Garden, Beiyuan Jiayuan, Chaoyang District, Beijing, China) were used to analysis oil contents of ODCs, biomass and their pyrolysis products.

2.3. Pyrolysis experiments

STA449F3 synchronous thermal analyzer (Netzsch Instruments Co., Germany) was used to study the sample weight loss process. Thermodynamic analysis of the samples was divided into two parts (1) individual pyrolysis and (2) co-pyrolysis, during both of which nitrogen was used as the protective gas (0.5 L/min). Samples of ODCs, biomass, and mixtures in different ratios, 30 g per test, were heated from 20°C to 1,000°C at various heating rates (5, 10, 20, and 30°C/min). The sample weight changes were measured continuously.

The fixed bed reaction device (VTL1200, Nanjing Bo Yun Tong Instrument Technology Co., Ltd., No. 7 Shijing Road, Gaoqiao Industrial Park, Jiangning District, Nanjing, China) for pyrolysis analysis contained a heating unit, a condensation recovery unit, an anti-back suction unit and an exhaust gas absorption unit. 30 g samples (ODCs, biomass) were used in each fixed bed reaction test to investigate four factors: final temperature of pyrolysis, remaining time final temperature



Fig. 1. Samples of ODCs (a) and biomass (b). ODCs were black solid blocks with a thick texture and emitted a strong diesel smell. The biomass was brown with no smell.

Table 1
Factors and gradients of fixed bed reaction tests

Gradient	Final pyrolysis temperature (°C)	Remaining time of final temperature (min)	Heating rate (°C/min)	N ₂ flow rate (L/min)
1	200	30	5	0.10
2	250	45	10	0.15
3	300	60	15	0.20
4	350	75	20	0.25
5	400	90		0.30
6	500			

time, heating rate, and nitrogen flow rate (Table 1). Since the maximum heating rate of the tube furnace was 20°C/min, there were only four gradients of heating rates.

3. Results and discussion

3.1. Characterization of samples

The CHNS/O elemental analysis (Table 2) shows that the main components of the ODCs are inorganic substances, like C, H, O, N, and S are both in low proportions. In contrast, biomass is organic, and these five elements together account for 83.22%. The H/C value of biomass is 37% greater than ODCs, which provides theoretical feasibility for the “co-hydrogen” effect.

XRF spectrum analysis (Table 3) and plasma emission spectroscopic analysis (Table 4) illustrated that ODCs samples are rich in silicon-aluminum compounds, and their pyrolysis residue can be used to produce building materials and road cushions. Compared with biomass, the content of alkali metals in ODCs is higher, which may act as a catalyst during co-pyrolysis to reduce the activation energy.

3.2. Thermogravimetry analysis

3.2.1. Individual pyrolysis of ODCs and biomass

Pyrolysis of ODCs and biomass was carried out using a simultaneous thermal analyzer. Fig. 2 shows the TG,

differential thermogravimetry (DTG), and differential scanning calorimetry (DSC) curves of ODCs and biomass heated from room temperature (20°C) to 1,000°C with a heating rate of 10°C/min. The DTG curve in Fig. 2a indicates that the pyrolysis process of ODCs can be roughly divided into three stages: (1) 20°C–400°C, involving the evaporation of external water, combined with evaporation of water and petroleum organic compounds [39], with a significant weight loss peak at 185°C; (2) 400°C–800°C, with a smaller loss peak at 467°C, due to the thermal decomposition of macromolecular hydrocarbons in the ODCs into small molecular compounds, and then escape from the system; (3) 800°C–1,000°C, there are two obvious weight loss peaks at 843°C and 915°C, as calcite, calcium carbonate, and other carbonates are pyrolyzed at high temperature [40]. In Fig. 2a, the DSC curve increases gradually from 100°C to 400°C, indicating continuous absorption of heat. From 400°C to 700°C, the volatiles are burned out, and the curve is only slightly higher than the baseline. At 800°C–900°C, an endothermic peak appears, which corresponds to the weight loss peak of the DTG curve. The DTG curve in Fig. 2b shows that the biomass loses weight slowly (3.32%) from 20°C to 200°C, attributing to internal water precipitation and glass transition. The maximum mass reduction is at 200°C–500°C, where hemicellulose and lignin are decomposed, and the weight loss reaches 60.00%. At 500°C–1,000°C, the weight loss rate slows down, with a 9.58% mass reduction, due to fixed carbon burnout and biomass carbonization [41]. The DSC curve changes

Table 2
CHNS/O elemental analysis of experimental materials

Content (%)	C	H	O	N	S
ODCs	13.54	1.14	6.38	0.10	2.36
Biomass	49.94	5.74	26.83	0.62	0.09

Table 3
Experimental material X-ray fluorescence spectrum analysis (%)

Content (%)	ODCs	Biomass
Na ₂ O	0.44	–
MgO	1.036	0.101
Al ₂ O ₃	6.863	0.023
SiO ₂	54.223	0.201
P ₂ O ₅	0.101	0.145
SO ₃	4.258	0.162
K ₂ O	1.398	1.108
CaO	3.749	0.087
TiO ₂	0.29	–
MnO	–	0.017
Fe ₂ O ₃	2.358	0.037
NiO	0.015	–
CuO	0.014	–
ZnO	0.018	–
As ₂ O ₃	0.003	–
Rb ₂ O	0.006	0.001
SrO	0.075	–
Y ₂ O ₃	0.003	–
BaO	1.54	–
PbO	0.011	–
Cl	1.212	0.455
Loss on ignition	22.368	97.661

Table 4
Plasma emission spectroscopic analysis of experimental materials (mg/kg)

Elements	ODCs	Biomass
Al	44,027.9	479.4
B	7.2	10.8
Ba	6,909.4	13.3
Be	1.7	0.3
Bi	534.0	121.9
Cd	5.0	0.3
Co	9.9	1.2
Cr	149.3	41.9
Cu	152.6	28.8
Fe	20,485.4	485.4
Li	–	387.3
Mg	5,685.1	783.1
Mn	116.2	156.2
Ni	82.2	9.9
Pb	127.4	–
Sb	35.5	–
Sn	14.7	6,060.3
Sr	293.9	10.5
Ti	1,124.6	31.3
V	285.4	–
Zn	258.8	41.1
Ca	22,263.0	1,351.2
K	10,788.9	12,911.3
Na	5,303.5	1,658.7
P	–	798.1
S	16,674.3	868.2
Zr	37.9	18.9
Si	–	952.0

correspond to this trend, with three endothermic peaks appearing at 73°C, 123°C, and 942°C, and an exothermic peak corresponding to the main weight loss range at 786°C.

The samples of ODCs and biomass were heated from 20°C to 1,000°C at a heating rate of 5, 10, 20, and 30°C/min. In Fig. 3 and the following statement, OB represents ODCs/biomass, with the first pair of appended numbers indicating the weight ratio of the two materials (e.g., OB10 is 100% ODCs with 0% biomass, and OB28 is 20% ODCs with 80% biomass). The number after the hyphens represents the heating rates (e.g., OB10-5 is OB10 heated at a rate of 5°C/min). Figs. 3a and c show the TG and DTG curves of the ODCs and biomass at different heating rates. With the increase of pyrolysis temperature, the weight loss rate of ODCs increases continuously, while the total weight loss rate is similar at different heating rates, and therefore the shapes of TG curves are similar, except at 30°C/min. However, there are significant differences in the shape among DTG curves: higher heating rates result in peaks curves that are more pronounced and shift to higher temperatures. A reasonable explanation is that when the heating rate is high, there is not enough time for

ODCs to absorb the heat and be fully pyrolyzed, thus the pyrolysis can only be completed at a higher temperature. As shown in Figs. 3b and d, the pyrolysis behavior of biomass at different heating rates are similar to that of ODCs. The heating rate mainly affects the shape of the DTG curve, which is determined by the rate of weight loss. In addition, the pyrolysis and coke products vary with the heating rate, owing to variations in the instantaneous rate of product precipitation.

3.2.2. Co-pyrolysis of ODCs and biomass

The effect of the mixing ratio on co-pyrolysis was analyzed by comparing the TG and DTG curves at seven mixing ratios of ODCs and biomass and a heating rate of 10°C/min. The solid curves in Fig. 4 show the experimental results of samples OB10, OB82, OB73, OB55, B 37, OB28, and OB01, and the dashed curves show the corresponding calculated values (CV10, etc.). Higher biomass content leads to greater weight loss at the end of pyrolysis (Fig. 4a), and faster weight loss at 200°C–450°C (Fig. 4b). When the ODCs/biomass ratios are higher than 5:5, the DTG curves of the mixed samples become similar to ODCs.

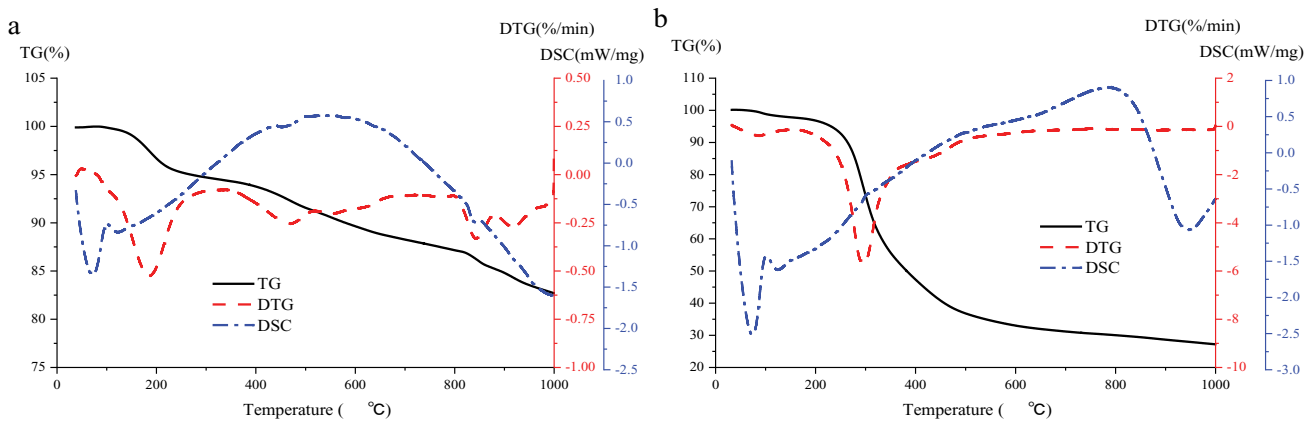


Fig. 2. TG, DTG, and DSC curves of ODCs (a) and biomass (b).

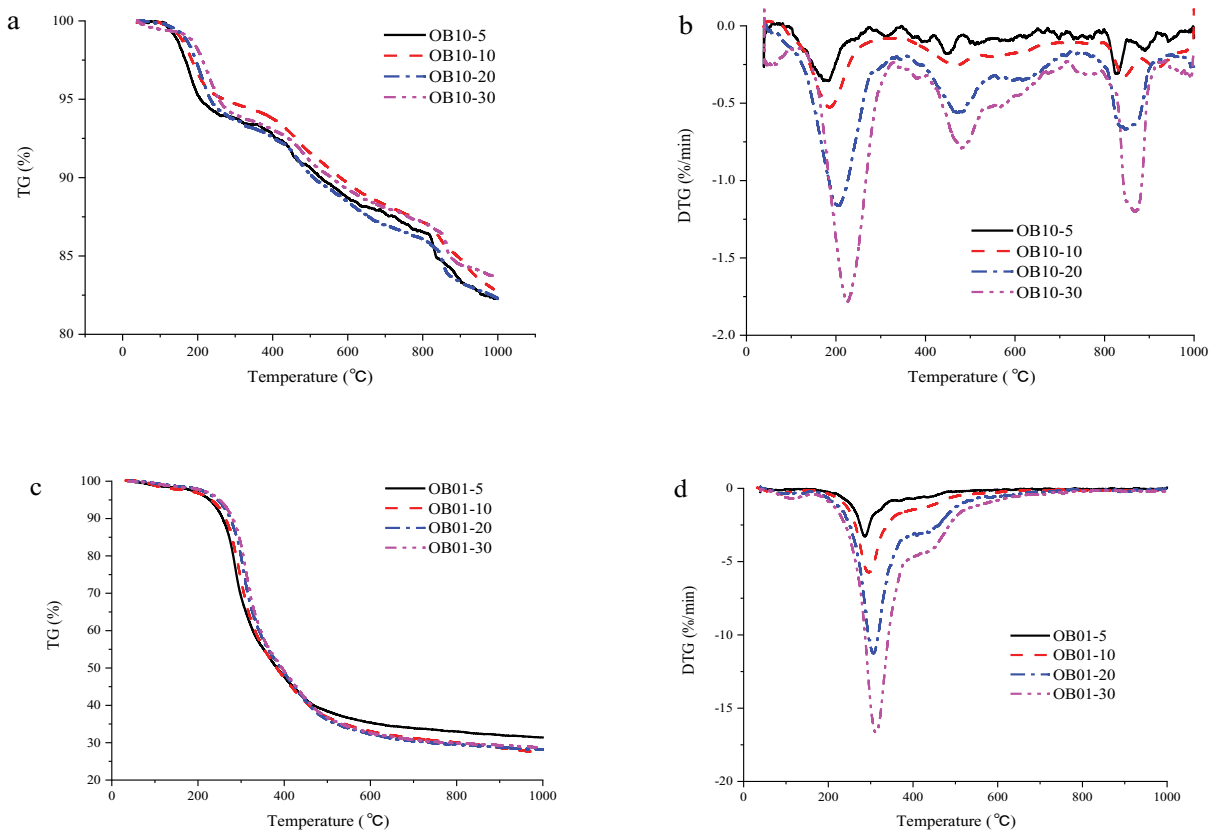


Fig. 3. TG and DTG curves of ODCs (a,c) and biomass (b,d) at different heating rates.

The pyrolysis temperatures in Fig. 4 can be divided into three ranges: (1) 20°C–450°C, (2) 450°C–750°C, and (3) 750°C–1,000°C. From the comparison of experimental and calculated thermogravimetric (CTG) and DTG curves, it can be seen that the experimental and calculated weight loss behaviors of the mixed pyrolysis are basically consistent in the middle-temperature range. However, in the low-temperature range, a significant deviation of DTG curves can be seen in OB82 and OB73. In the high-temperature range, the decomposition peaks appear in the experimental curves

of samples OB82 and OB73, which do not exist in the calculated curves. However, the calculation curves of the samples with higher biomass content, namely OB55, OB37 and OB28, are almost the same as the experimental curves, with no significant weight loss peaks in the high-temperature range. In addition, a phenomenon of biomass enveloping ODCs during heating can be observed, and a higher biomass ratio results in a more fully enveloping, which might be a possible explanation for the poor co-pyrolysis performance of samples with low OB ratios.

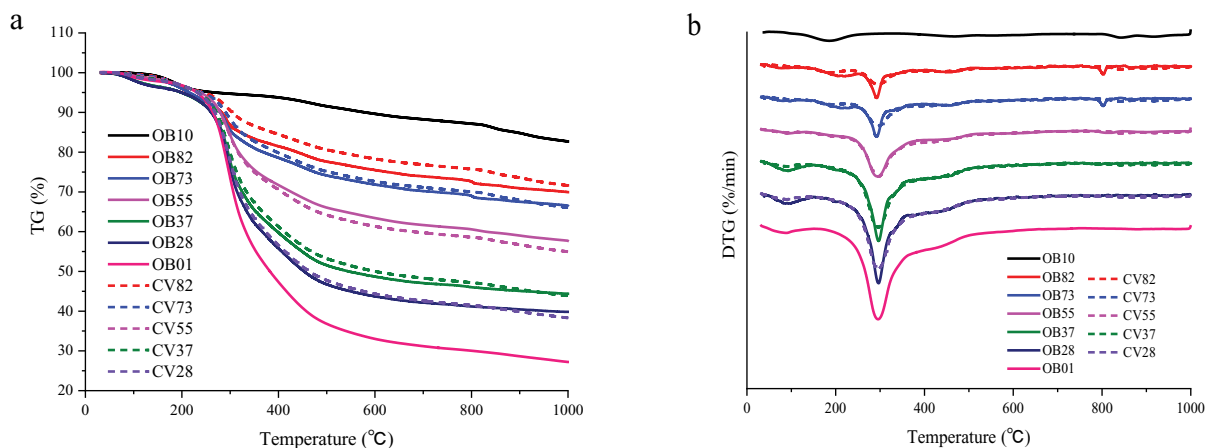


Fig. 4. Comparison between calculated and actual TG curves (a) and DTG curves (b) for co-pyrolysis at different mixing ratios (heating rate 10°C/min).

The characteristic parameters of pyrolysis reflect the stability of the test samples. The initial precipitation temperature reflects the stability of the internal structure of the sample, which is a sign that large molecules are cleaved in the sample to produce small molecules; the temperature corresponding to the maximum rate of weight loss provides a reflection of the stability of the sample; and the lower the cut-off temperature, the higher the activity of the sample [13]. The TG curves do not change significantly with heating rate, except for the lowest rate of 5°C/min (Fig. 5a). From the DTG curves, it can be seen that in low and high-temperature ranges, the weight loss peak shifts to a higher temperature and widens as the heating rate increases, because the samples quickly reach the precipitation cut-off temperature and the particle surface pyrolysis gas cannot be taken out at high heating rates. There are deviations between the calculated and experimental DTG curves, and the experimental values of the temperature corresponding to the maximum weight loss rate are lower than the calculated values, indicating that the co-pyrolysis of ODCs and biomass involves advantageous synergistic effects.

3.3. Fixed bed pyrolysis analysis

3.3.1. Effect of different pyrolysis parameters in fixed bed reaction

ODCs, biomass and their 5:5 mixtures were pyrolyzed under different conditions separately (Fig. 6). When one factor was examined in each test, the other pyrolysis parameters were: pyrolysis temperature 350°C, remaining time 60 min, heating rate 10°C/min, N₂ flow rate 0.15 L/min.

Pyrolysis temperature and remaining time were more conducive to a higher reduction of residual oil content, which was consistent with the general knowledge. The heating rate affected the heat and mass transfer inside the particles. In general, under low heating rates, samples could be fully preheated and pyrolyzed thoroughly. However, at the heating rate of 20°C/min, the reaction of biomass was intensified, and a large amount of pyrolysis gas accumulated in the reactor to cause a secondary cracking reaction. As a

result, the oil contents of biomass and mixture decreased instead. Besides, appropriate nitrogen flow can take the pyrolysis gas out of the reaction system in time to promote the reaction forward.

Considering the oil content of pyrolysis residue and liquid yield, the optimal pyrolysis conditions are as below: pyrolysis temperature 350°C, remaining time 60 min, heating rate 10°C/min, N₂ flow rate 0.15 L/min. Under this condition, the oil content of each sample can be reduced to less than 3,000 mg/kg. This is lower than the maximum allowable content of mineral oil specified in the Control Standards of Pollutants in Sludge for Agricultural Use 4284-84, which is currently used by the Jiangnan Oilfield of the Fuling Shale Gas Co., Ltd., to control the treated slag oil content of ODCs.

3.3.2. Analysis of pyrolysis products under different mixing ratios

In order to further study the co-pyrolysis effects and mechanism of ODCs and biomass, we chose five mixing ratios (OB82, OB73, OB55, OB37, OB28) and pure ODCs (OB10), biomass (OB01) for pyrolysis under optimal conditions (Fig. 7). When the ODCs and biomass were mixed at a ratio of 3:7 (OB37), minimum oil content of the pyrolysis residue was obtained (1,414.80 mg/kg); after the ratio increased to 7:3 (OB73), the synergistic effect between ODCs and biomass was optimized, as the actual oil content in the pyrolysis residue differed greatly from the calculated value (up to 425.50 mg/kg, 21.71%). The mutual promotion between ODCs and biomass increases first and then decreases with the increase of biomass ratio.

The pyrolysis liquid products were analyzed by GC-MS with carbon tetrachloride as extractant. In order to analyze the reaction process of ODCs and biomass at different ratios, the components of each sample were divided into hydrocarbons, aldehydes, ketones, phenols, alcohols, furans, esters, acids, and other types (Fig. 8). According to their stability, flammability, and pollutant discharge, these components can be divided into favorable groups (hydrocarbons, ketones, esters, alcohols, furans) and harmful groups (aldehydes, phenols, acids and other types) [42,43]. Using the content of each substance in the liquid products

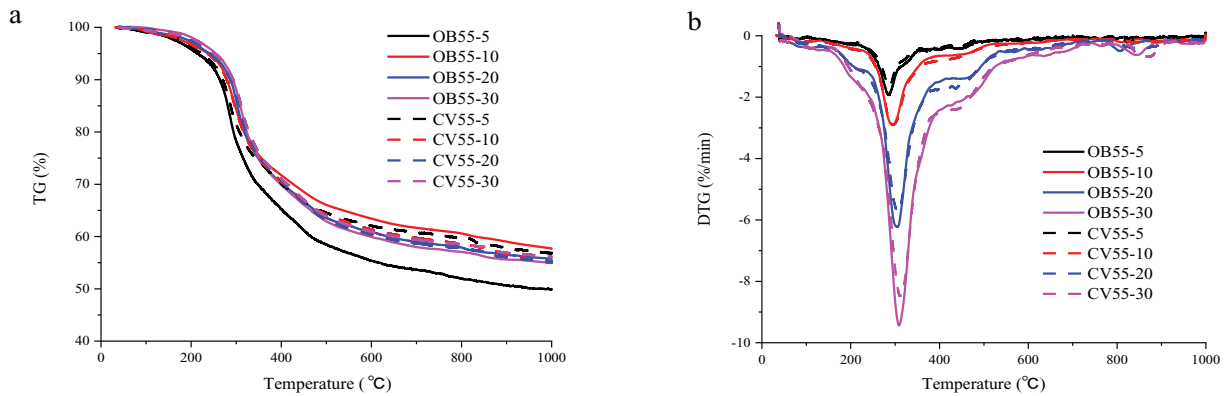


Fig. 5. Comparison between calculated and actual TG curves (a) and DTG curves (b) at different heating rates for mixed samples with a 5:5 mixing ratio.

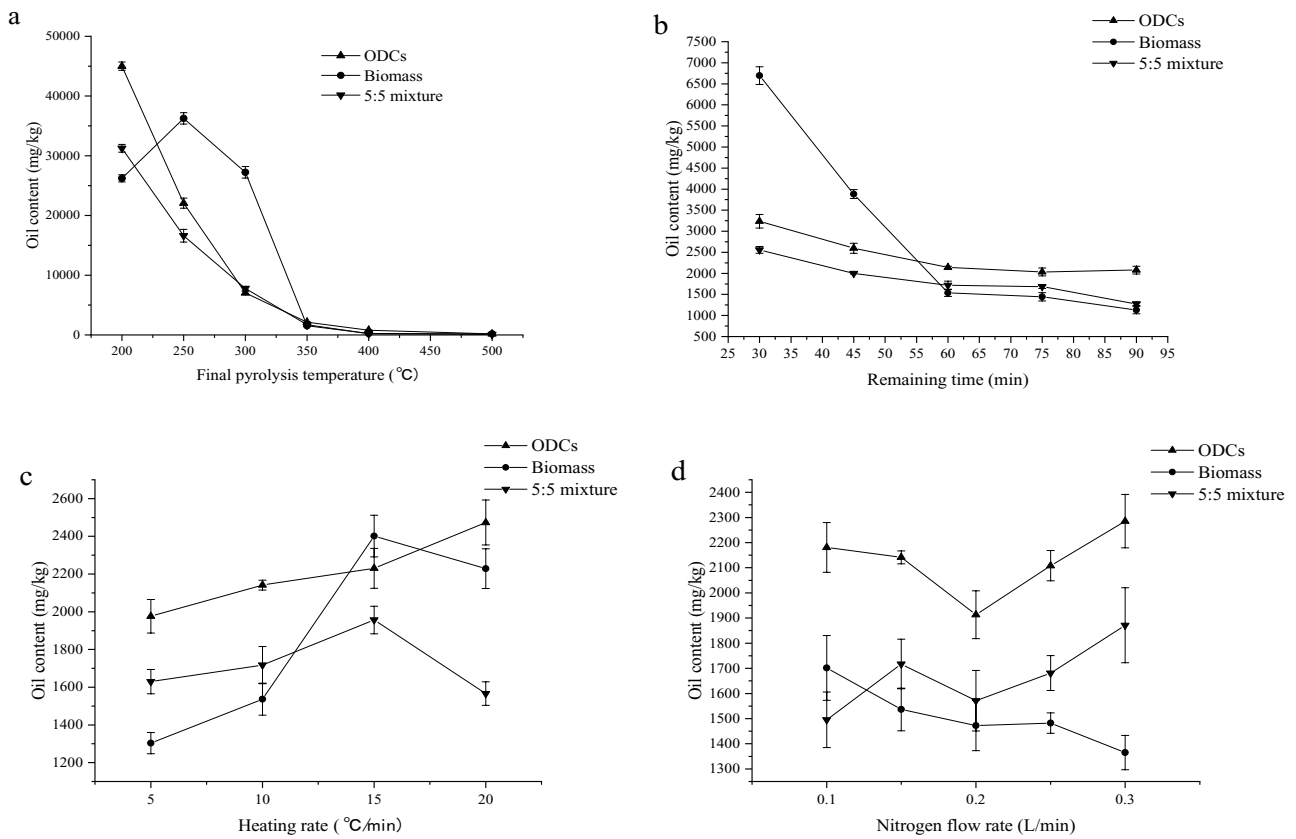


Fig. 6. Impacts of final pyrolysis temperature, remaining time, heating rate and nitrogen flow rate on pyrolysis efficiency, valued by oil content of residues.

of ODCs and biomass (separately pyrolyzed), the calculated value of each substance was obtained by weighted average according to the mixing ratio, then subtract the calculated value from the actual value to obtain Table 5. The positive value data in the table indicates that the actual value of this substance is greater than the calculated value—means that co-pyrolysis promotes the generation of this substance, while the negative value is the opposite. Since the

main products of ODCs pyrolysis are hydrocarbons, and biomass is aldehydes, the content of these two substances is also the highest during co-pyrolysis. It can be seen that appropriate mix ratios (OB82, OB73) can significantly promote the formation of hydrocarbons and inhibit the formation of aldehydes, which is good for further processing and utilization. This proves that the co-pyrolysis of the two can promote each other to produce better liquid yields.

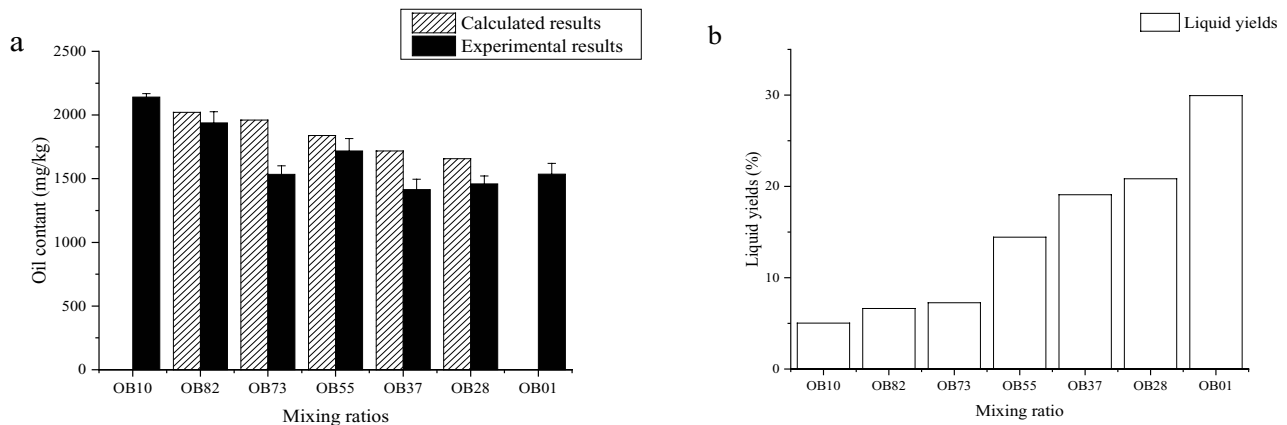


Fig. 7. Effect of mixing ratio on the oil content of pyrolysis residue (a) and liquid yields (b).

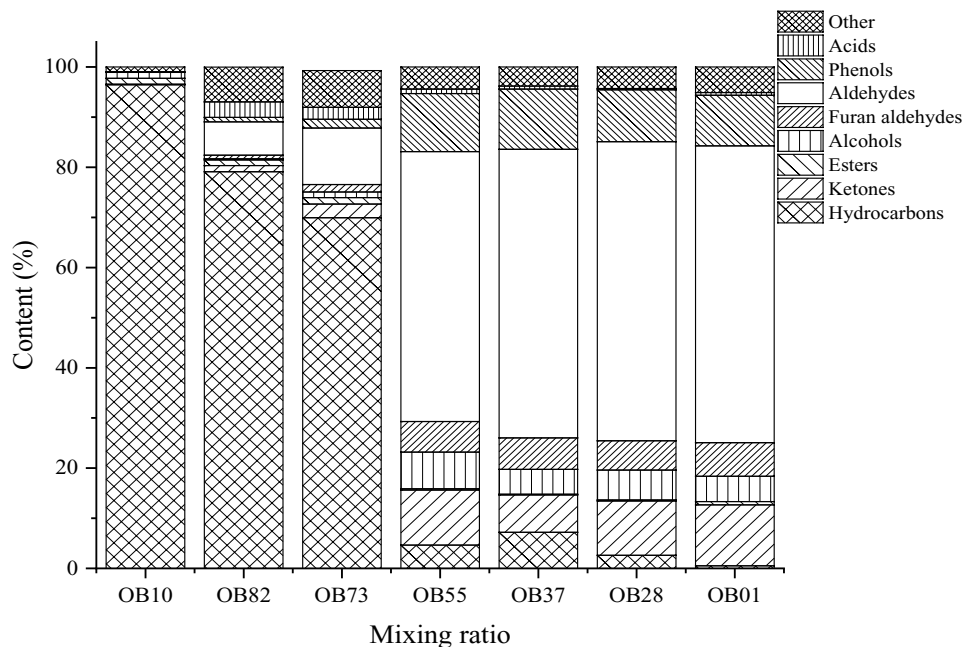


Fig. 8. Composition of liquid phase produced by pyrolysis of samples with different mixing ratios.

Table 5
Differences between the actual and calculated values of the liquid products from ODCs and biomass co-pyrolysis

	OB82	OB73	OB55	OB37	OB28
Hydrocarbons	1.86	2.26	-43.85	-22.10	-17.12
Ketones	-1.29	-0.98	4.87	-1.09	1.13
Esters	0.05	0.25	-0.67	-0.67	-0.58
Alcohols	-1.72	-1.21	4.18	1.07	1.68
Furan aldehydes	-0.63	-0.53	2.77	1.58	0.50
Aldehydes	-5.20	-6.48	24.24	16.13	12.28
Phenols	-1.13	-1.29	6.53	4.94	2.27
Acids	2.87	2.12	0.53	0.20	-0.21
Other	5.18	5.15	1.40	-0.06	0.04

3.4. Proposed mechanism of co-pyrolysis

3.4.1. The effects posed on ODCs from biomass

Due to the nature of the structure and composition of the biomass, the addition of biomass to the ODCs can both promote or inhibit the pyrolysis. The specific mechanism of action is proposed as follows:

3.4.1.1. Promoting the pyrolysis of ODCs by H in biomass

According to the theory of coal chemistry, if a hydrogen atom can be assigned to a carbon atom during coal pyrolysis, it can be volatilized together. In the coal chemical industry, hydrothermal pyrolysis of coal can improve pyrolysis efficiency, oil product quantity and quality. Similarly, biomass has a high H/C ratio, which can satisfy the needs of its own

carbon atoms, and excess hydrogen can be used as a hydrogen donor for the pyrolysis of ODCs. When ODCs and biomass are co-pyrolyzed, hydrogen in the biomass may be transferred to the ODCs, thereby promoting the pyrolysis of the ODCs.

3.4.1.2. Inhibition of pyrolysis of ODCs by physical properties of biomass

As the density of biomass is much smaller than that of ODCs, for these two substances of equal mass, biomass is much bigger than ODCs. Also, biomass will soften and deform during pyrolysis. Therefore, when the biomass is added too much, the ODCs are completely wrapped during pyrolysis. As the amount of biomass added increases, a large amount of volatiles of the biomass evaporates, cover and adhere to the surface of the ODCs, block the pores, and inhibit the volatilization of the ODCs.

3.4.2. The effects posed on biomass by ODCs

3.4.2.1. Catalytic action of alkali metal oxides on pyrolysis of biomass in ODCs

The content of alkali metal, (K, Ca, Na, etc.) in the ODCs is higher than that of the biomass (Table 2), which has positive effects on liquid and gas yield during biomass pyrolysis [44]. Therefore, the addition of ODCs to the biomass may have a certain catalytic effect on the pyrolysis of the biomass.

3.4.2.2. Inhibition of pyrolysis of ODCs on biomass pyrolysis

The ODCs contain a considerable amount of petroleum substances, which precipitate from about 200°C, lower than the main pyrolysis temperature of the biomass. Their precipitation produces various hydrocarbon gas, which cannot be brought out from the heating system in time by the carrier gas, therefore hinders the biomass pyrolysis. So excessive ODCs may inhibit the pyrolysis of biomass.

3.5. Kinetics of the co-pyrolysis process analysis

Based on a function-free model, the ODCs and biomass mixture were subjected to kinetic analysis at multiple heating rates. The FWO, non-model method was used to obtain the preliminary results of activation energy, and the Coats–Redfern integration method (model-fitting method) was used to infer the mechanism function describing the TG process in a certain temperature range [45,46].

The sample pyrolysis conversion rate α (the degree of decomposition) is given by:

$$\alpha = \frac{m_0 - m_t}{m_0 - m_\infty} \times 100\% \quad (1)$$

where m_0 is the initial sample mass, m_t is the instantaneous sample mass, and m_∞ is the sample mass at the end of the reaction at 1,000°C. The decomposition rate equation is:

$$\frac{d\alpha}{dt} = k_f(\alpha) \quad (2)$$

where the Arrhenius rate constant is given by:

$$k = A \exp\left(-\frac{E}{RT}\right) \quad (3)$$

where A is the pre-exponential factor (min^{-1}), E is the reaction activation energy (kJ/mol), $R = 8.314 \times 10^{-3}$ kJ/(mol K) is the ideal gas constant, and T is the reaction temperature (K). From Eqs. (2) and (3), the total reaction equation for pyrolysis is:

$$\frac{d\alpha}{dt} = A \exp\left(-\frac{E}{RT}\right) f(\alpha) \quad (4)$$

Under non-isothermal conditions, the pyrolysis heating rate can be expressed as:

$$\beta = \frac{dT}{dt} \quad (5)$$

Eq. (4) then becomes:

$$\frac{d\alpha}{dT} = \frac{A}{\beta} \exp\left(-\frac{E}{RT}\right) f(\alpha) \quad (6)$$

3.5.1. Model-free methods: FWO

The FWO model, an integral technique which considers that the apparent activation energy remains constant throughout the reaction, is represented by Eq. (7), by applying integration to Eq. (6):

$$g(\alpha) = \int_0^\alpha \frac{d\alpha}{f(\alpha)} = \left(\frac{A}{\beta}\right) \int_{T_0}^T \exp\left(-\frac{ER}{T}\right) dT = \left[\frac{AE}{\beta R}\right] P(u) \quad (7)$$

where $P(u) = \int_\infty^u \frac{e^{-u}}{u^2} du$, $u = \frac{E}{RT}$, and $g(\alpha)$ is an integral form of reaction model.

Eq. (8) was given by using Doyle’s approximation and inserting the logarithm on both sides of Eq. (7), also called as FWO equation:

$$\log\beta = \log\left(\frac{AE}{Rg(\alpha)}\right) - 2.135 - 0.4567 \frac{E}{RT} \quad (8)$$

Therefore, a plot of $\log(\beta)$ vs. $1/T$, considering different heating rates, generates parallel lines for different conversions. The slopes of these straight lines are proportional to the activation energy E .

Biomass and 5:5 mixture have good liner fits ($R^2 > 0.93$) for $\alpha < 0.6$ (Figs. 9b and c), except for $\alpha = 0.1$ of mixture, which may be caused by experimental error. ODCs can only be fitted when $\alpha \leq 0.2$, and higher α leads to a rapid decline in the goodness of fit (Fig. 9a). Table 6 shows the reaction activation energy (E) given by slopes in Fig. 9.

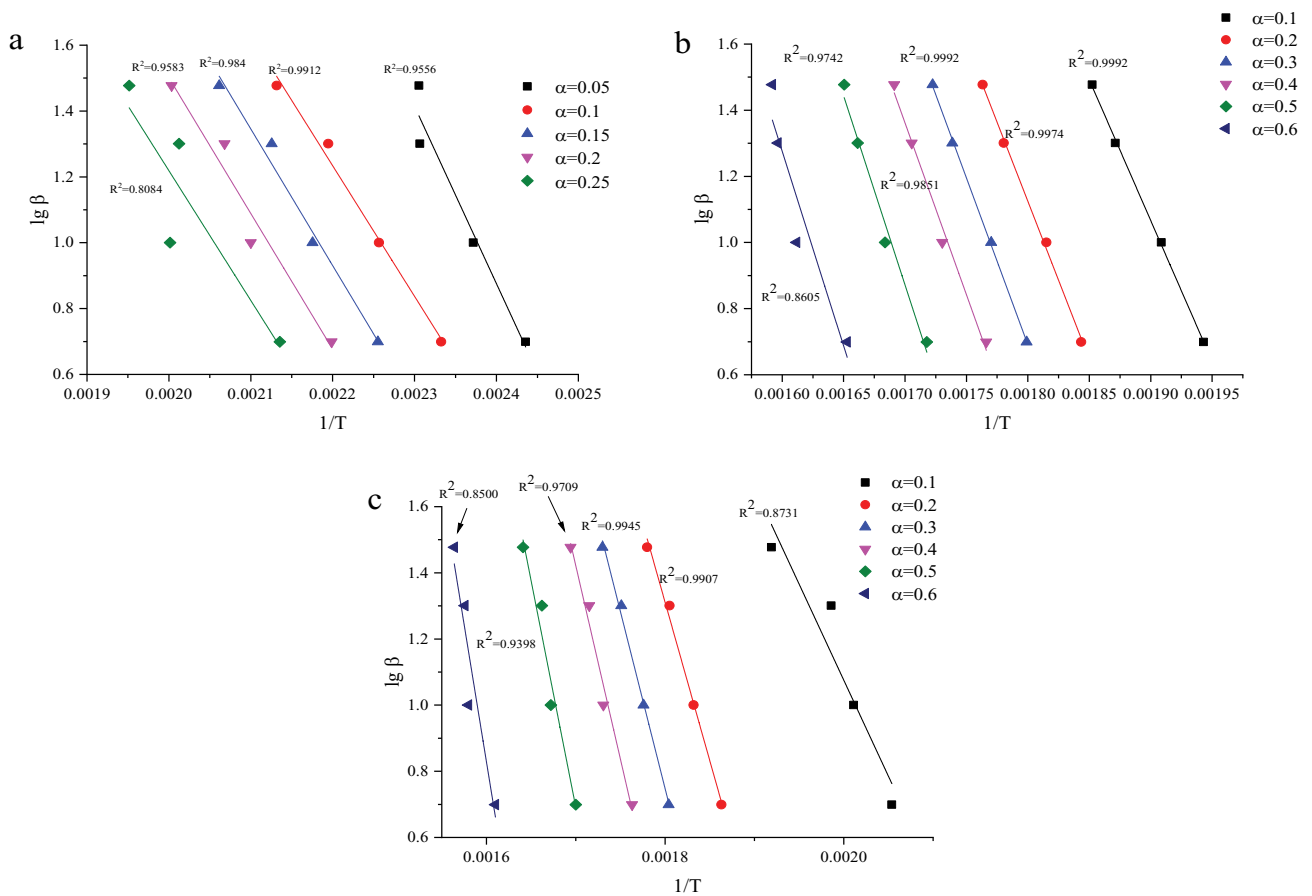


Fig. 9. Liner plots of $\log\beta-1/T$ for ODCs (a), biomass (b) and 5:5 mixture (c) under different conversion rates.

Table 6
Activation energy of ODCs, biomass and 5:5 mixtures under different conversion rates, given by FWO method

ODCs		Biomass		Mixtures	
α	E (kJ/mol)	α	E (kJ/mol)	α	E (kJ/mol)
0.05	98.02	0.05	113.08	0.05	64.45
0.1	72.22	0.1	154.88	0.1	105.77
0.15	75.57	0.15	169.90	0.15	158.76
0.2	75.05	0.2	173.85	0.2	174.25
		0.25	179.25	0.25	186.36
		0.3	183.59	0.3	194.81
		0.35	186.27	0.35	202.14
		0.4	189.07	0.4	213.07
		0.45	195.37	0.45	236.77
		0.5	208.20	0.5	249.22
		0.55	214.01	0.55	258.65
Average	80.22	Average	178.86	Average	185.84

3.5.2. Model-fitting method: Coats–Redfern

The basic equation for coats and Redfern method is given as:

$$\ln \frac{g(\alpha)}{T^2} = \ln \frac{AR}{\beta E} \left(1 - \frac{2RT}{E} \right) - \frac{E}{RT} \tag{9}$$

Because $\frac{2RT}{E} \ll 1$ Eq. (9) can be simplified as follows:

$$\ln \frac{g(\alpha)}{T^2} = \ln \left(\frac{AR}{\beta E} \right) - \frac{E}{RT} \tag{10}$$

where $g(\alpha)$ is a kinetic function of different reaction mechanisms that is obtained from the integration of $f(\alpha)$. Activation energy can be obtained by drawing a graph between $1/T$ and

$\ln \frac{g(\alpha)}{T^2}$. The pre-exponential factor can be obtained from the

intercept of this graph. $g(\alpha)$ can be varied according to the different developed models and reaction mechanisms. Most of the solid-state degradation reactions fall into five categories which are listed below in Table 7. Under the heating rate of 5°C, for $\alpha < 0.2$ (ODCs) or $\alpha < 0.6$ (biomass and 5:5 mixture), we use those reaction models to calculate active energy (E), pre-exponential factor (A) and goodness of fit (R^2) (Table 8). Nucleation and growth are considered as the most suitable model for ODCs ($N_{1/2}$), biomass ($N_{1/3}$) and mixture ($N_{1/4}$), as it has high R^2 values (>0.94) and similar E with those given by FWO method.

Under the heating rate of 5°C/min, for $\alpha < 0.2$ (ODCs) or $\alpha < 0.6$ (biomass and 5:5 mixture), we used the reaction models in Table 6 to calculated their active energy (E), pre-exponential factor (A) and goodness of fit (R^2). As the activation energy given by FWO method is 80.22 kJ/mol (ODCs), 178.86 kJ/mol (biomass), 185.84 kJ/mol (mixture), the nucleation and growth is considered as the most suitable model to fit those samples: $N_{1/2}$ for ODCs, $N_{1/3}$ for biomass and $N_{1/4}$ for the mixture. $N_{1/4}$ was also employed for CTG fitting.

In order to verify the effects of co-pyrolysis on active energy, we used a CTG getting from the 5:5 weighted average of ODCs and biomass TG curves, then it was fitted using nucleation and growth model under four different heating rates together with other three samples (Table 9). Compared to CTG, the active energy of 5:5 mixture was lower at heating rates of 5, 10 and 20°C/min, only slightly higher at 30°C/min, and the average active energy was 146.74 kJ/mol (CTG), 142.82 kJ/mol (mixture), respectively. At $\alpha < 0.6$, the temperature ranges for mixture and CTG are both around 20°C–350°C, corresponding to the best pyrolysis temperature discussed in section 3.2 (thermogravimetry analysis). Therefore, we concluded that the co-pyrolysis of ODCs and biomass produced a favorable synergy effect.

4. Conclusion

In order to solve the problem of ODCs recycling and biomass utilization, this paper carries out separate pyrolysis

Table 7 Expressions for the reaction mechanisms and its integrated form in solid-state reactions

	Reaction order	Boundary controlled reaction	Power law	Nucleation and growth	Diffusion
$f(\alpha)$	O_0	R_2	P_1	$N_{1/2}$	D_1
$g(\alpha)$	O_1	R_3	P_2	$N_{1/3}$	D_2
Hypothesis	$(1-\alpha)^n$ α Decomposition of particles by random nucleation and growth does not exceed single-crystal nucleation.	$(1-\alpha)^{(1-1/n)}$ $1-(1-\alpha)^{1/2}$ Based on initial fast densification nucleation on the crystal plane. Tight spacing results in a rapid reaction zone that advances at a constant rate without diffusion effects.	$n(\alpha)^{(1-1/n)}$ $\alpha^{1/3}$ The power law of nucleation is based on accelerating the nucleation process and requires several different steps to generate the growth nucleus.	$n(1-\alpha)[- \ln(1-\alpha)]^{(1-1/n)}$ $[- \ln(1-\alpha)]^2$ The model is also based on an accelerated nucleation process, but also considers the dimension of nuclear growth.	$1/2\alpha$ α^2 The diffusion model is based on a reaction in which the transport of reactants or products from chemically altered sites can be controlled by a diffusion process if the transport is slower than the chemical step.

Table 8
Summary of activation energy calculated by Coats–Redfern method

Model name	ODCs			Biomass			5:5 Mixture		
	<i>E</i> (kJ/mol)	<i>A</i>	<i>R</i> ²	<i>E</i> (kJ/mol)	<i>A</i>	<i>R</i> ²	<i>E</i> (kJ/mol)	<i>A</i>	<i>R</i> ²
O ₀	41.1800734	1,351.1439	0.9913	45.4252018	454.50977	0.9834	25.536451	3.6989879	0.969
O ₁	44.1107584	3,479.8903	0.9933	53.6452536	3,948.7144	0.9831	30.703602	17.065047	0.9587
R ₂	42.6292036	1,079.3258	0.9924	49.3859914	646.91775	0.9839	28.026494	3.8837556	0.9644
R ₃	43.1197296	842.88709	0.9927	50.7727666	620.7401	0.9838	28.897801	3.3488529	0.9626
P ₁	4.90592512	0.0353908	0.9578	4.64079166	0.0178302	0.9071	–	–	–
P ₂	8.9367186	0.1643792	0.9779	9.1720048	0.0844503	0.9558	2.7324792	0.0063803	0.7943
N _{1/2}	95.411464	1.364E+09	0.9944	116.246348	2.254E+09	0.9853	70.077043	73,031.607	0.9665
N _{1/3}	146.70053	3.798E+14	0.9947	178.842454	9.139E+14	0.986	109.45381	213,886,270	0.9685
N _{1/4}	197.99791	9.285E+19	0.9949	241.446874	3.249E+20	0.9683	148.8206	5.455E+11	0.9695
D ₁	89.54178	221,372,571	0.9927	99.801256	35,752,585	0.9862	59.74191	4,229.27	0.976
D ₂	91.454	200,412,533	0.9933	104.897738	64,905,200	0.9864	62.945294	5,140.0514	0.9733

Table 9
Model-fitting results of ODCs, biomass, 5:5 mixture and CTG at different heating rates

	5°C/min			10°C/min			20°C/min			30°C/min		
	<i>E</i> (kJ/mol)	<i>A</i> (min ⁻¹)	<i>R</i> ²	<i>E</i> (kJ/mol)	<i>A</i> (min ⁻¹)	<i>R</i> ²	<i>E</i> (kJ/mol)	<i>A</i> (min ⁻¹)	<i>R</i> ²	<i>E</i> (kJ/mol)	<i>A</i> (min ⁻¹)	<i>R</i> ²
ODCs (N _{1/2})	95.41	1.36E+9	0.9944	83.86	2.06E+7	0.9934	95.77	2.86E+8	0.9996	77.72	1.18E+6	0.9859
Biomass (N _{1/3})	178.84	9.14E+14	0.986	171.38	8.52E+13	0.9841	194.66	6.58E+15	0.9607	198.86	1.16E+16	0.9890
Mixture (N _{1/4})	127.31	2.18E+9	0.9695	126.55	1.1E+9	0.9436	140.52	1.67E+10	0.9607	176.91	3.27E+13	0.9697
CTG (N _{1/4})	127.78	3.04E+9	0.9607	134.06	5.22E+9	0.9515	154.22	1.84E+10	0.9744	170.91	9.98E+12	0.9823

and co-pyrolysis, compares the pyrolysis effects, and judges whether the two can produce mutually synergy effect. The following main conclusions can be drawn:

- The pyrolysis process of ODCs can be divided into three stages. (1) 20°C–400°C, involving precipitation of water and petroleum-based organic matter; (2) 400°C–800°C, where large-molecule hydrocarbons break down into small-molecule compounds; (3) 800°C–1,000°C, where carbonates breakdown.
- When ODCs and biomass are individually pyrolyzed and co-pyrolyzed, as the heating rate increases, the DTG peaks are shifted to a higher temperature and widened, resulting in pyrolysis hysteresis. A comparison of the calculated values for mixed pyrolysis at different heating rates with the actual values indicates that co-pyrolysis produces a favorable synergy in the low and high-temperature ranges.
- The pyrolysis effect increases with the rise of the final pyrolysis temperature and the remaining time of the final pyrolysis temperature. The optimal pyrolysis process parameters are pyrolysis temperature of 350°C, remaining time of 60 min, a heating rate of 10°C/min, a nitrogen flow rate of 0.15 L/min. Under these conditions, the oil contents of all samples pyrolysis ash are lower than 3,000 mg/kg, specified in GB 4284-1984.
- When the biomass blending ratio is 30%, the oil content of pyrolysis ash shows the most significant decrease

rate compared to the calculated value. Also, when the ODCs ratio is 70%, 80%, co-pyrolysis can reduce harmful components and increase favorable components in liquid products.

- The activation energy for ODCs, biomass and 5:5 mixture pyrolysis was calculated by the model-free and model-fitting method. The average activation energy of the mixture obtained from experimental data is lower than the calculated value at 20°C–350°C, indicating that the co-pyrolysis of ODCs and biomass has a favorable synergistic effect.

Acknowledgment

This research was supported by the Fuling Shale Gas Environmental Exploration Technology of National Science and Technology Special Project (Grant No. 2016ZX05060).

References

- [1] C.-q. Wang, X.-y. Lin, M. He, D. Wang, S.-l. Zhang, Environmental performance, mechanical and microstructure analysis of concrete containing oil-based drilling cuttings pyrolysis residues of shale gas, *J. Hazard. Mater.*, 338 (2017) 410–427.
- [2] H. Liu, J.B. Li, M. Zhao, Y.B. Li, Y.M. Chen, Remediation of oil-based drill cuttings using low-temperature thermal desorption: performance and kinetics modeling, *Chemosphere*, 235 (2019) 1081–1088.

- [3] C.-q. Wang, J.-z. Jin, X.-y. Lin, D.-m. Xiong, X.-d. Mei, A study on the oil-based drilling cutting pyrolysis residue resource utilization by the exploration and development of shale gas, *Environ. Sci. Pollut. Res.*, 24 (2017) 17816–17828.
- [4] S. Wang, C.C. Zheng, J.H. Zhao, X.J. Li, H.S. Lu, Extracting and recovering diesel from oil-based drill cuttings using switchable hydrophilic solvents, *Chem. Eng. Res. Des.*, 128 (2017) 27–36.
- [5] Y. Ye, J.X. Li, Q.W. Zhang, J.Y. Feng, J.Z. Zhu, D. Yin, Nanoemulsion for oil-contaminated oil-based drill cuttings removal in lab, *Int. J. Hydrogen Energy*, 42 (2017) 18734–18740.
- [6] R. Khanpour, M.R. Sheikhi-Kouhsar, F. Esmailzadeh, D. Mowla, Removal of contaminants from polluted drilling mud using supercritical carbon dioxide extraction, *J. Supercrit. Fluids*, 88 (2014) 1–7.
- [7] N. Alavi, A.-R. Mesdaghinia, K. Naddafi, G. Mohebbali, H. Daraei, A. Maleki, L. Alaei, Biodegradation of petroleum hydrocarbons in a soil polluted sample by oil-based drilling cuttings, *Soil Sediment Contam.: Int. J.*, 23 (2014) 586–597.
- [8] R.B. Kogbara, B.B. Dumkhana, J.M. Ayotamuno, R.N. Okparanma, Recycling stabilised/solidified drill cuttings for forage production in acidic soils, *Chemosphere*, 184 (2017) 652–663.
- [9] J.P. Robinson, S.W. Kingman, C.E. Snape, R. Barranco, H. Shang, M.S.A. Bradley, S.M. Bradshaw, Remediation of oil-contaminated drill cuttings using continuous microwave heating, *Chem. Eng. J.*, 152 (2009) 458–463.
- [10] P. Yan, M. Lu, Y.M. Guan, W.M. Zhang, Z.Z. Zhang, Remediation of oil-based drilling cuttings through a biosurfactant-based washing followed by a biodegradation treatment, *Bioresour. Technol.*, 102 (2011) 10252–10259.
- [11] W. Huang, Z. Zhou, Y. He, M. Yan, S. Xia, Resources utilization of oil-based drilling cuttings vacuum pyrolysis in shale gas developing, *Chin. J. Environ. Eng.*, 8 (2017) 4783–4788.
- [12] Z.Q. Wang, Q.J. Guo, X.M. Liu, C.Q. Cao, Low temperature pyrolysis characteristics of oil sludge under various heating conditions, *Energy Fuels*, 21 (2007) 957–962.
- [13] J.W. Yan, X.M. Jiang, X.X. Han, J.G. Liu, A TG–FTIR investigation to the catalytic effect of mineral matrix in oil shale on the pyrolysis and combustion of kerogen, *Fuel*, 104 (2013) 307–317.
- [14] Y.J. Hu, W.J. Yu, H. Wibowo, Y.Y. Xia, Y.J. Lu, M. Yan, Effect of catalysts on distribution of polycyclic-aromatic hydrocarbon (PAHs) in bio-oils from the pyrolysis of dewatered sewage sludge at high and low temperatures, *Sci. Total Environ.*, 667 (2019) 263–270.
- [15] L. Ding, Y.Q. Zhang, Z.Q. Wang, J.J. Huang, Y.T. Fang, Interaction and its induced inhibiting or synergistic effects during co-gasification of coal char and biomass char, *Bioresour. Technol.*, 173 (2014) 11–20.
- [16] J.H. Clark, F.E.I. Deswarte, Introduction to Chemicals from Biomass, John Wiley & Sons Ltd., 2015.
- [17] P. Basu, Biomass Gasification, Pyrolysis and Torrefaction: Practical Design and Theory, Academic Press, 2018.
- [18] V. Dhyani, T. Bhaskar, A comprehensive review on the pyrolysis of lignocellulosic biomass, *Renewable Energy*, 129 (2018) 695–716.
- [19] F.-X. Collard, J. Blin, A review on pyrolysis of biomass constituents: mechanisms and composition of the products obtained from the conversion of cellulose, hemicelluloses and lignin, *Renewable Sustainable Energy Rev.*, 38 (2014) 594–608.
- [20] M. Sharifzadeh, C.J. Richard, K. Liu, K. Hellgardt, D. Chadwick, N. Shah, An integrated process for biomass pyrolysis oil upgrading: a synergistic approach, *Biomass Bioenergy*, 76 (2015) 108–117.
- [21] K. Açıklan, F. Karaca, E. Bolat, Pyrolysis of pistachio shell: effects of pyrolysis conditions and analysis of products, *Fuel*, 95 (2012) 169–177.
- [22] E. Mura, O. Debono, A. Villot, F. Paviet, Pyrolysis of biomass in a semi-industrial scale reactor: study of the fuel-nitrogen oxidation during combustion of volatiles, *Biomass Bioenergy*, 59 (2013) 187–194.
- [23] L. Baxter, Biomass-coal co-combustion: opportunity for affordable renewable energy, *Fuel*, 84 (2005) 1295–1302.
- [24] C.C. Zhou, G.J. Liu, X.D. Wang, C.C. Qi, Co-combustion of bituminous coal and biomass fuel blends: thermochemical characterization, potential utilization and environmental advantage, *Bioresour. Technol.*, 218 (2016) 418–427.
- [25] G.W. Wang, J.L. Zhang, J.G. Shao, Z.J. Liu, G.H. Zhang, T. Xu, J. Guo, H.Y. Wang, R.S. Xu, H. Lin, Thermal behavior and kinetic analysis of co-combustion of waste biomass/low rank coal blends, *Energy Convers. Manage.*, 124 (2016) 414–426.
- [26] M.V. Navarro, J.D. Martínez, R. Murillo, T. García, J.M. López, M.S. Callén, A.M. Mastral, Application of a particle model to pyrolysis. Comparison of different feedstock: plastic, tyre, coal and biomass, *Fuel Process. Technol.*, 103 (2012) 1–8.
- [27] R.M. Soncini, N.C. Means, N.T. Weiland, Co-pyrolysis of low rank coals and biomass: product distributions, *Fuel*, 112 (2013) 74–82.
- [28] A.O. Aboiyade, J.F. Görgens, M. Carrier, E.L. Meyer, J.H. Knoetze, Thermogravimetric study of the pyrolysis characteristics and kinetics of coal blends with corn and sugarcane residues, *Fuel Process. Technol.*, 106 (2013) 310–320.
- [29] F. Abnisa, W.M.A. Wan Daud, A review on co-pyrolysis of biomass: an optional technique to obtain a high-grade pyrolysis oil, *Energy Convers. Manage.*, 87 (2014) 71–85.
- [30] Z.Q. Wu, S.Z. Wang, J. Zhao, L. Chen, H.Y. Meng, Synergistic effect on thermal behavior during co-pyrolysis of lignocellulosic biomass model components blend with bituminous coal, *Bioresour. Technol.*, 169 (2014) 220–228.
- [31] G. Agarwal, B. Lattimer, Physicochemical, kinetic and energetic investigation of coal–biomass mixture pyrolysis, *Fuel Process. Technol.*, 124 (2014) 174–187.
- [32] S.L. Rowan, F. Wu, I.B. Celik, N.T. Weiland, Experimental investigation of char generated from co-pyrolysis of coal and Appalachian hardwoods, *Fuel Process. Technol.*, 128 (2014) 354–358.
- [33] S.G. Sahu, N. Chakraborty, P. Sarkar, Coal–biomass co-combustion: an overview, *Renewable Sustainable Energy Rev.*, 39 (2014) 575–586.
- [34] J. Kalemkiewicz, U. Chmielarz, Ashes from co-combustion of coal and biomass: new industrial wastes, *Resour. Conserv. Recycl.*, 69 (2012) 109–121.
- [35] G.K. Parshetti, A. Quek, R. Betha, R. Balasubramanian, TGA–FTIR investigation of co-combustion characteristics of blends of hydrothermally carbonized oil palm biomass (EFB) and coal, *Fuel Process. Technol.*, 118 (2014) 228–234.
- [36] B.C. Lin, Q.X. Huang, Y. Chi, Co-pyrolysis of oily sludge and rice husk for improving pyrolysis oil quality, *Fuel Process. Technol.*, 177 (2018) 275–282.
- [37] J. Shao, Study on Synergy of Co-Pyrolysis of Lignin Alkaline and Oil Shale, Dissertation of Master, Northeast Dianli University, 2016. Available at: <http://kns.cnki.net/KCMS/detail/detail.aspx?dbcode=CMFD&dbname=CMFD201602&filename=1016183096.nh&v=MDI5MzBSbUZ5L2hVcnJkVjYyNkdMS3dIZEhGcVpFYlBJUjhlWDFMdXhZUZdEaDFUM3FUcldNMUZYQlVSTEtWlXU=> (accessed May 29, 2018)
- [38] W.R. Shi, X.Z. Wang, C.M. Zhang, A.G. Feng, Z.S. Huang, Experimental study on gas content of adsorption and desorption in Fuling shale gas field, *J. Pet. Sci. Eng.*, 180 (2019) 1069–1076.
- [39] C. Chen, S.Q. Li, C.T. Yue, T. Kruttschnitt, E. Pruckner, Q. Yao, Lab-scale pyrolysis of oil sludge in continuous rotating reactor: mass/energy balance and product analysis, *J. Chem. Ind. Eng. (China)*, 3 (2006) 650–657.
- [40] B. Sun, P. Tan, C. Jia, H. Liu, Q. Wang, Study on the combustion process of oil shale by DSC, *J. Northeast Dianli Univ. (Natural Science Edition)*, 28 (2008) 105–108.
- [41] A.A. Salema, R.M.W. Ting, Y.K. Shang, Pyrolysis of blend (oil palm biomass and sawdust) biomass using TG-MS, *Bioresour. Technol.*, 274 (2019) 439–446.
- [42] Z. Song, Z. Zhong, B. Zhang, Z. Lv, K. Ding, Experimental study on catalytic co-pyrolysis of corn stalk and polypropylene, *J. Zhejiang Univ. (Engineering Edition)*, 50 (2016) 333–340.
- [43] A.K. Hossain, P.A. Davies, Pyrolysis liquids and gases as alternative fuels in internal combustion engines – a review, *Renewable Sustainable Energy Rev.*, 21 (2013) 165–189.

- [44] M.S. Masnadi, R. Habibi, J. Kopyscinski, J.M. Hill, X.T. Bi, C.J. Lim, N. Ellis, J.R. Grace, Fuel characterization and co-pyrolysis kinetics of biomass and fossil fuels, *Fuel*, 117 (2014) 1204–1214.
- [45] S.R. Naqvi, R. Tariq, Z. Hameed, I. Ali, M. Naqvi, W.-H. Chen, S. Ceylan, H. Rashid, J. Ahmad, S.A. Taqvi, M. Shahbaz, Pyrolysis of high ash sewage sludge: kinetics and thermodynamic analysis using Coats–Redfern method, *Renewable Energy*, 131 (2019) 854–860.
- [46] M. Fernandez-Lopez, G.J. Pedrosa-Castro, J.L. Valverde, L. Sanchez-Silva, Kinetic analysis of manure pyrolysis and combustion processes, *Waste Manage.*, 58 (2016) 230–240.